2D Materials

Determination of the elastic moduli of CVD graphene by probing graphene/polymer Bragg stacks

2D Materials

PAPER

Determination of the elastic moduli of CVD graphene by probing graphene/polymer Bragg stacks

Bohai Liu[1,2], Christos Pavlou[3,4], Zuyuan Wang[2,6], Yu Cang[5], Costas Galiotis[3,4,*] and George Fytas[2,*]

[1] Center for Phononics and Thermal Energy Science, China-EU Joint Center for Nanophononics, School of Physics Science and Engineering, Tongji University, Shanghai 200092, People's Republic of China
[2] Max Planck Institute for Polymer Research, Ackermannweg 10, 55128 Mainz, Germany
[3] Institute of Chemical Engineering Sciences, Foundation of Research and Technology-Hellas (FORTH/ICE-HT), Stadiou Street, 26504 Platani, Patras, Greece
[4] Department of Chemical Engineering, University of Patras, 26504 Patras, Greece
[5] School of Aerospace Engineering and Applied Mechanics, Tongji University, 100 Zhangwu Road, Shanghai 200092, People's Republic of China
[6] Institute for Measurement and Automation, Division of Sensor Technology and Measurement Systems, Bundeswehr University Munich, Werner-Heisenberg-Weg 39, 85579 Neubiberg, Germany
* Authors to whom any correspondence should be addressed.

E-mail: c.galiotis@iceht.forth.gr, galiotis@chemeng.upatras.gr and fytas@mpip-mainz.mpg.de

Keywords: CVD graphene, elastic/shear moduli, Brillouin light spectroscopy, wrinkles, poly(methyl methacrylate), Bragg stacks

Supplementary material for this article is available online

OPEN ACCESS

RECEIVED
8 January 2021

REVISED
7 April 2021

ACCEPTED FOR PUBLICATION
7 May 2021

PUBLISHED
26 May 2021

Abstract

Graphene has been widely used in the form of micro-flakes to fabricate composite materials with enhanced mechanical properties. Due to the small size of the inclusions and their random orientation within the matrix, the superior mechanical properties of graphene cannot be fully exploited. Recently, attempts have been made to fabricate nanolaminate composites by interleaving large sheets of chemical vapor deposition (CVD) monolayer graphene between thin layers of polymer matrices. However, CVD graphene is inevitably accompanied by wrinkles that are formed in the synthesis process, and it remains unknown how the wrinkles affect the mechanical properties of graphene. Here, we employ Brillouin light spectroscopy to study the elastic moduli of CVD graphene by probing graphene/poly(methylmethacrylate) hybrid Bragg stacks at zero strain. We find the Young's and shear moduli of the CVD graphene, which has wrinkles in the form of sharp elevations with a height of about 6 nm and a fullwidth at half maximum (FWHM) of ca. 30 nm, to be 680 $\pm$ 16 and 290 $\pm$ 10 GPa, respectively, with the former being about 30% lower than that of exfoliated, flat graphene. This work sheds light on the elastic properties of CVD graphene and provides a method that can be extended to studying the wrinkle-induced softening effect in other two-dimensional materials.

1. Introduction

The unique hexagonal sp^2 C–C bonds endow graphene with remarkable physical properties, including extremely high thermal conductivity [1], electron mobility [2], and intrinsic strength [3]. Ever since its first fabrication by mechanical exfoliation [4], graphene has attracted extensive attention in the materials research community. For the mechanical properties, exfoliated suspended graphene has a Young's modulus of 1 $\pm$ 0.1 TPa, and a breaking strength of 42 N m^{-1} [3]. On the theoretical side, a Young's modulus of 1050 GPa and a tensile strength of 110 GPa were reported [5].

The superior mechanical properties of graphene have made it an ideal filler to reinforce polymer materials [6–9]. To realize reliable functional materials, mass production and large-scale integration of graphene are prerequisites. Fortunately, chemical vapor deposition (CVD) has emerged as a promising solution [10–12], which perfectly satisfies the requirements and has been widely applied in graphene-based

composites [13, 14]. However, multiple grain boundaries and atomic defects in CVD graphene can deteriorate its properties [15], such as the intrinsic strength, as the motion of dislocations is interrupted by these defects [16]. Furthermore, due to the thermal expansion mismatch between graphene and the copper substrate, severe biaxial stresses are developed on CVD graphene as it cooled from approximately 1000 °C down to ambient temperature. These stresses are relaxed by the formation of a network of folds that form a mosaic structure as seen in many atomic force microscopy (AFM) images [17, 18]. Additionally, CVD graphene typically replicates the topography of the substrate. All of these can often introduce out-of-plane wrinkles [19–22].

The elastic properties of CVD graphene have been theoretically and experimentally investigated. Theoretically, it has been shown that wrinkles play a dominant role in softening CVD graphene membranes [23]. The wrinkle-induced effect has been experimentally measured by Raman spectroscopy [24] and nanoindentation using AFM [25]. The latter addresses a small area under the AFM tip, and the highly nonuniform strain distribution over the sample can result in large spatial fluctuations of the two-dimensional elastic modulus. The former determines the strain-induced shift of the characteristic G and 2D Raman peaks of graphene [26, 27], and this allows the estimation of the elastic modulus via the Gruneisen parameters and the Poisson's ratio of the substrate [28]. For CVD graphene, however, the Raman wavenumber shifts with strain for both G and 2D peaks are markedly lower than those obtained from exfoliated graphene which indicate that the CVD modulus must be lower than the quoted modulus of ∼1 TPa for monolayer graphene [27].

Despite the several aforementioned studies on the elastic properties of CVD graphene, a comprehensive understanding of the wrinkle-induced softening effect on the elasticity is still lacking. To tackle this problem, noncontact measurements of large-area CVD graphene appear to be an effective way for a quantitative study, particularly at zero strain. To the best of our knowledge, no such study has been reported in the literature. As a non-contact, non-destructive technique, Brillouin light spectroscopy (BLS) detects thermally excited phonons in the gigahertz range, whose frequencies are directly related to the elastic moduli. It has been utilized to determine the elastic modulus of laminated materials, including poly(methyl methacrylate) (PMMA)/SiO_2 Bragg stacks [29], clay/polymer Bragg stacks [30], and polycarbonate/PMMA (PC/PMMA) multilayer films [31]. Here, we employ BLS to study the wrinkle-introduced effect on the elastic moduli of CVD graphene by probing CVD graphene/PMMA (Gr/PMMA) Bragg stacks. From the BLS measurements, we directly obtained the sound velocities of the longitudinal acoustic (LA) phonons for both PMMA and the Gr/PMMA stacks. We conducted phononic band structure calculations using the Young's modulus of the CVD graphene as an adjustable parameter. We also performed tensile tests to compute the stiffness of the Gr/PMMA stacks in the axial direction at moderate strains and compared the results with those from the BLS experiments.

2. Methods

2.1. Preparation and characterization of CVD Gr/PMMA multilayer stacks

Graphene growth was performed in a commercial CVD reactor (AIXTRON Black Magic Pro, Germany) on 7 cm × 7 cm copper sheets (JX Nippon Mining & Metals, 35 μm thick, 99.95%). The produced graphene on the copper foil of dimensions 20 mm × 35 mm was coated with PMMA solution in anisole (495 PMMA, Microchem) to produce PMMA solid films via spin coating [32]. The spinning conditions and the solution concentrations, listed in table 1, were optimized accordingly to produce the desired thickness of the Gr/PMMA films. Then, the sample was allowed to float on a 0.15 M aqueous etchant solution of ammonium persulphate (APS) to etch away the copper substrate. After copper etching, the floating Gr/PMMA membrane was thoroughly rinsed with deionized-double distilled water until the APS solution was fully replaced. Then the floating film was deposited on another Gr/PMMA layer on a copper foil (which serves as the sacrificial substrate for the repetitive film depositions) by removing the water, as detailed elsewhere [32]. The deposited film was dried at 40 °C for several hours, and then it was post-baked at 150 °C for 5 min on a hot plate. This procedure was repeated until the desired number of layers was achieved. To separate the Gr/PMMA stacks from the copper substrate, a similar APS solution was used as described above. We prepared three samples with different graphene volume fractions, which are labeled as Gr(0.2)/PMMA, Gr(3.3)/PMMA, and Gr(5.1)/PMMA, respectively. The number of stacking periods and the corresponding volume fraction of graphene are shown in table 1.

2.2. BLS

It is well known the elastic modulus is coupled with the acoustic sound velocity near the Γ point in the first Brillouin zone [33, 34]. In this study, we applied BLS to determine the sound velocity of the Gr/PMMA Bragg stacks. In a typical BLS experiment, the phonon wave vector $\boldsymbol{q} = \boldsymbol{k}_s - \boldsymbol{k}_i$, where $\boldsymbol{k}_s$ and $\boldsymbol{k}_i$ is the wave vector of the scattered and incident light, respectively. A laser with a wavelength of 532 nm was utilized to probe the phonons, and the scattered light was detected by a six-pass tandem Fabry–Perot interferometer. The LA phonon can be observed in the VV spectra, where V denotes a vertical polarization with respect to the scattering plane defined by $\boldsymbol{k}_i$ and $\boldsymbol{k}_s$.

Table 1. Structural characteristics of the three Gr/PMMA Bragg stacks.

Specimen code	Number of PMMA layers	Thickness of one PMMA layer (nm)	Solution wt%	RPM	Volume fraction of graphene (%)
Gr(0.2)/PMMA	6	1500	11	3000	0.02
Gr(3.3)/PMMA	15	100	2	1000	0.33
Gr(5.1)/PMMA	25	66	2	2000	0.51

Using a VV polarization configuration, we conducted measurements in the transmission (with a scattering angle, $\theta = 90°$) and backscattering geometries to detect the LA phonon mode in the in-plane (parallel to the sample films) and cross-plane (normal to the sample films) directions, respectively. Because of light absorption [35], graphene can convert part of the incident light energy to heat, which can lead to melting of PMMA and even burning of the stacks. To avoid any hotspot, we installed a filter in front of the specimens to control the incident power, which was measured by an optical power meter (Newport Model 1961 C).

2.3. Tensile test

Tensile tests were performed on a micro-tensile tester equipped with a 5 N load cell (MT-200, Deben UK Ltd, Woolpit, UK). The specimens were strips of dimensions of 35 mm × 1 mm in length and width, respectively. The thickness of the films was evaluated using a digital micro-meter with a resolution of 0.1 μm (Mitutoyo, Japan). The mean film thickness was calculated based on ten measurements within the gauge length area. During the tensile test, the two ends of the strip were fixed to a 25 mm × 25 mm paper frame by using a two-part cold curing epoxy resin. A paper frame was utilized to prevent any early failure within the gripping zone. The tests were carried out at room temperature at a strain rate of 0.008 min^{-1}. The stress and strain values were extracted from the recorded load and displacement raw data. The estimation of the Young's modulus was obtained by the mean values of at least ten samples for each graphene content, and the experimental errors are the deviation from the mean values. The analysis was performed by using linear regression of the initial linear part of the stress–strain curves.

2.4. Raman characterization

Raman mapping was performed on an area of 50 μm × 50 μm by acquiring spectra at steps of 2 μm. A Renishaw Invia Raman Spectrometer with 2400 and 1200 grooves mm^{-1} grating for the 514 nm laser excitation and a 100× lens with an numerical aperture (NA) of 0.85 and working distance (WD) of 1.0 was used to evaluate the quality of the Gr on macroscale nanolaminates. The laser power was kept below 1 mW to avoid overheating the specimens. All Raman peaks were fitted with Lorentzian functions, and the spectroscopic parameters (peak position and FWHM) were recorded at each position on the film.

3. Results

3.1. Characterization of the Gr/PMMA stacks

Figure 1(a) shows the AFM image of the investigated CVD graphene, which was placed on a Si/SiO_2 wafer surface by using the lift-off/float-on deposition process (figure S1 (available online at stacks.iop.org/2DM/8/035040/mmedia)). The wrinkles introduced by the synthesis process can be clearly seen in figure S5 by the AFM line scan, and correspond to sharp elevations of a maximum height of 6 nm and an average FWHM of ca. 30 nm. The stacks were then fabricated by the wet transfer method, and the corresponding SEM image of Gr(0.2)/PMMA is shown in figure 1(b). Raman spectroscopy and X-ray diffraction pattern (XRD) were employed to evaluate the quality of the graphene layers during the sample preparation. In figure 1(c), two representative spectra from single and multi Gr/PMMA layers are presented. It is evident that the G and 2D peak intensities for multi Gr/PMMA layers are higher due to the contribution of multiple graphene layers to the spectrum. As estimated from the Raman wavenumber contours in figure S2, after the first deposition, the 2D peak was found to be slightly blue shifted due to the compressive fields generated (around 0.04%, figure S3(a)) during the polymer thin film preparation [36]. The other spectroscopic characteristics of graphene spectrum correspond to typical values obtained from a single layer CVD graphene with an FWHM of ∼33 cm^{-1} for the 2D peak and an intensity ratio, $I(2D)/I(G)$, of ∼2.3 (figure S3(a)) [37, 38]. Raman spectra were acquired during each deposition, and only minor spectral changes were observed vis-a-vis the first deposition. In figure S3, the contours of 2D peak, the FWHM of 2D peak, and the $I(2D)/I(G)$ ratios are presented. A small broadening of the 2D peak may be attributed to the expected slight wavenumber variations between each graphene layer within the sampling volume [8]. According to a previous study, both G and 2D peaks undergo red-shift and their FWHMs can be broadened by increasing the average wrinkle height and their FWHMs as well [39]. The nearly unchangeable G and 2D peak positions with their FWHMs of Gr/PMMA stacks in our case indicate that no residual stresses are developed during the

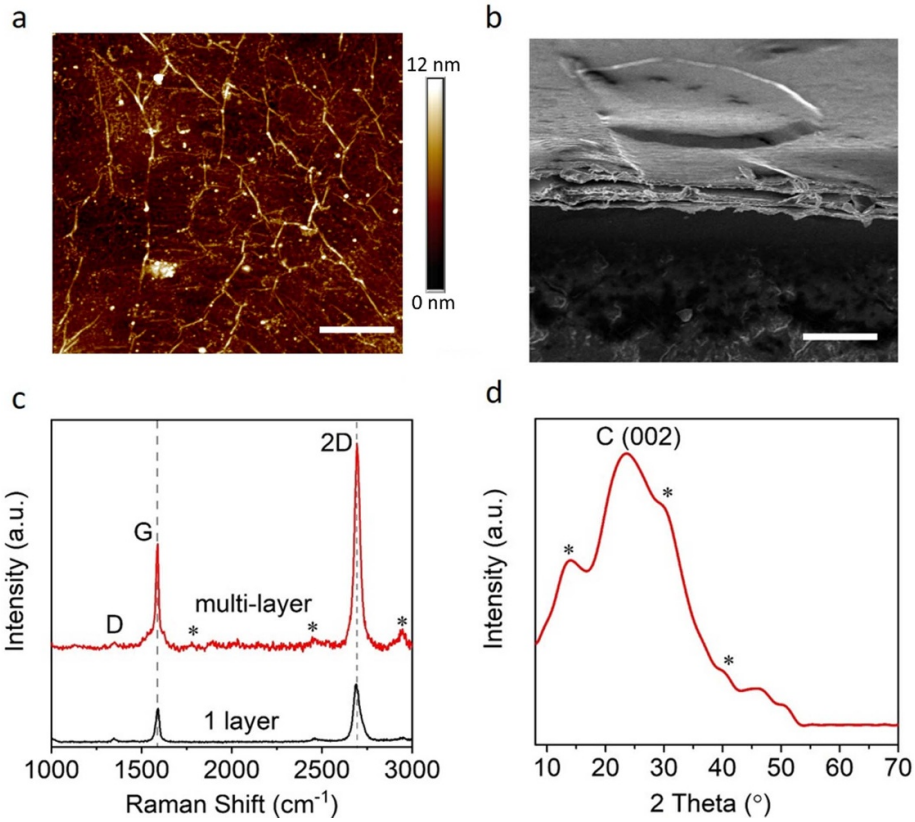

Figure 1. Characterization of the Gr/PMMA multilayer stacks. (a) AFM image of the CVD graphene with a maximum wrinkle height of ∼6 nm. The scale bar is 740 nm. (b) Side view of Gr/PMMA(0.2) under SEM where the lateral structure can be seen. The scale bar is 100 μm. (c) Representative Raman spectra collected from a single (bottom) and multiple (top) graphene/PMMA layers. Asterisks mark the spectroscopic features of PMMA. The vertical dashed lines mark the robust peak during the wet transfer (i.e. lift-on and float-off) process [41]. (d) XRD pattern for Gr/PMMA(0.2). The highest peak denotes the characteristic peak of graphene while the asterisks mark PMMA peaks.

wet transfer/ solidification process. Figure 1(d) displays the XRD pattern of Gr(0.2)/PMMA in the 2θ range from 10 to 70°, which apparently shows the characteristic peaks for both graphene and PMMA. Known as an amorphous polymer, PMMA has the three broad peaks at 2θ= 13.8°, 31.8° and 40°, in which the first reflects the ordered packing of polymer chains, and the second and third denotes the ordering inside the main chains, respectively [40]. The peak at $2\theta = 24°$ denotes the (200) face of graphene and the corresponding d-spacing is 3.7 Å. Upon multiple depositions of Gr/PMMA layers, a slight increase of the I(D)/I(G) ratio vis-à-vis a single Gr/PMMA layer is observed; revealing a minor inducement of structural defects by the sequential assembly of the Gr/PMMA hybrid Bragg stacks (figure S4). It is clear from the contours (figures S2 and S3) and the XRD pattern that the graphene quality was not seriously affected by the sample preparation since the spectral characteristics are similar to those obtained for the single layer.

3.2. Elastic modulus of CVD graphene from BLS

Figure 2 shows exemplary polarized BLS spectra (anti-Stokes side) of Gr(0.2)/PMMA recorded at a constant $\boldsymbol{q} = 0.0167\ \mathrm{nm}^{-1}$; the corresponding BLS spectra for pure PMMA, Gr(3.3)/PMMA, and Gr(5.1)/PMMA are shown in figures S6–S8. The peak position of the spectra defines the frequency of the longitudinal phonon referring to the effective medium acoustic phonon in the Gr/PMMA Bragg stack. As a dispersive medium, PMMA exhibits fast segmental dynamics at elevated temperatures well above its glass transition temperature (around 380 K). Under ambient conditions, the sound propagation is dissipation free [42]. Conversely, the sound velocity in Gr is nearly independent of temperature in the range of 300–500 K [43], which covers the local temperatures in our experiments. The relatively stable sound velocity of graphene allows us to measure it by probing the Gr/PMMA stacks. Therefore, the red shift of the LA frequency in the two scattering geometries is simply attributed to the decreasing sound velocity of PMMA with increasing laser power.

Figures 3(a) and (b) show the power-dependent longitudinal sound velocity in the in-plane ($c_{\mathrm{L},\parallel}$) and cross-plane ($c_{\mathrm{L},\perp}$) direction, respectively. For Gr(5.1)/PMMA, $c_{\mathrm{L},||} = \frac{2\pi f}{q}$, are 3070 and 2434 m s^{-1} at P = 1.66 and 6.85 mW, respectively. When the incident power exceeds a threshold, a sharper decrease of $c_{\mathrm{L},\parallel}$ is observed. By linear fitting of the

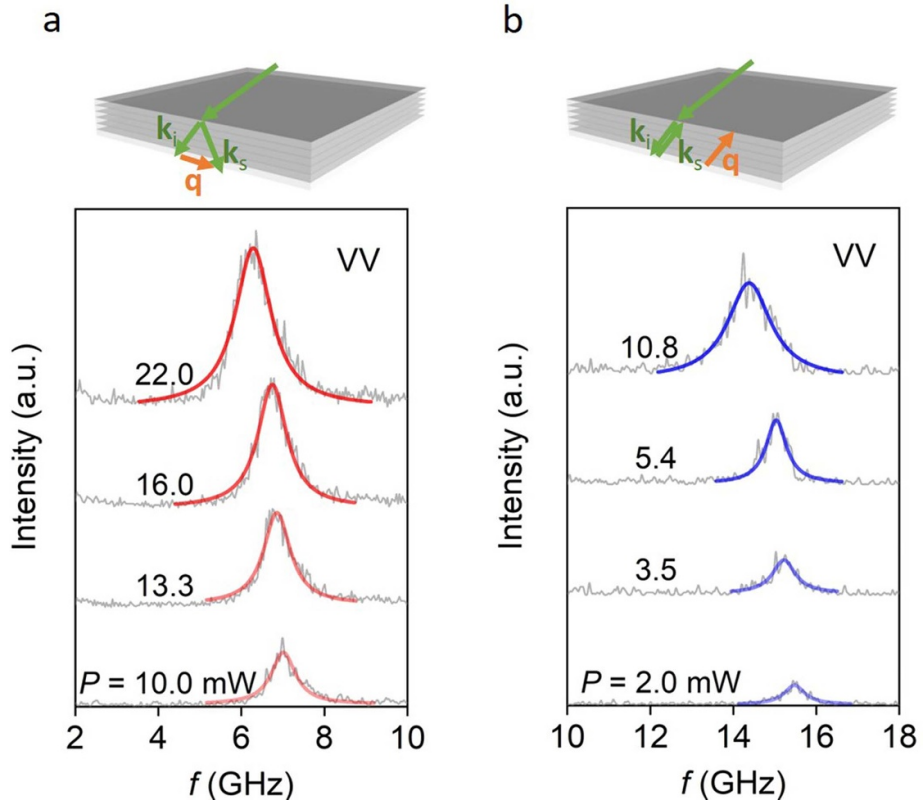

Figure 2. Brillouin light scattering spectra of Gr(0.2)/PMMA. The exemplary spectra recorded in the (a) transmission and (b) backscattering geometries are represented by single Lorentzian peaks (red and blue curves). VV denotes a vertical polarization configuration of the incident and scattered light with respect to the scattering plane of $\boldsymbol{k}_i$ and $\boldsymbol{k}_s$ (schemes in the top panels). At a higher incident power, a clear red shift of the peak position is observed in both geometries. In the schematics, the thermally excited phonons are probed by the incident light with a wave vector $\boldsymbol{k}_i$, and the scattered light has a wave vector $\boldsymbol{k}_s$. The phonon wave vector is $\boldsymbol{q} = \boldsymbol{k}_s - \boldsymbol{k}_i$. The grey and black sheets denote PMMA and CVD graphene layers, respectively.

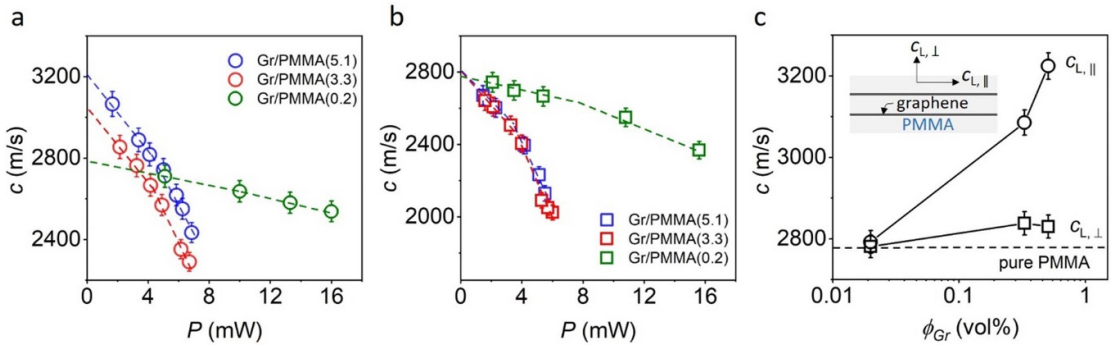

Figure 3. Longitudinal sound velocity, c_L of the CVD graphene/PMMA hybrid Bragg stacks. The variation of c_L, in-plane, and cross-plane phonon propagation with the incident laser power are shown in (a) and (b), respectively. The PMMA is in the glassy (rubbery) state at laser powers lower (higher) than the value at the kink. The intercepts (at $P = 0$ mW) of the linear fits to the data denote the sound velocities of the samples at 295 K. The dashed lines are linear fits to the data. (c) The effective in-plane $c_{L,\|}$ and cross-plane $c_{L,\perp}$ as shown schematically in the inset, are plotted as a function of the graphene volume fraction percentage. The circles (squares) data symbols denote the in-plane (cross-plane) c_L and the two lines are guide to the eye. The black dashed line represents the sound velocity of pure PMMA.

data before and after the sharp decrease, a kink is clearly seen. The kink is rationalized by the glass transition of PMMA [44], at which the phonon vibration undergoes an abrupt softening. At much higher temperatures, the velocity corresponds to the adiabatic zero frequency sound velocity, c_0, while at much lower temperatures it corresponds to the solid-like or 'infinite' frequency sound velocity, c_∞ [43] .Thus, the decrease rates of the $c_{L,\|}$ in Gr/PMMA with respect to temperature, are different in the glassy and rubbery states. The kink for Gr(0.2)/PMMA appears at $P = 8$ mW, whereas the kink positions for the other two samples are at much lower power levels, owing to the larger number of graphene layers (i.e. more light absorption in Gr(3.3)/PMMA and Gr(5.1)/PMMA than Gr(0.2)/PMMA); the sound velocity of the fully

transparent PMMA is expectedly robust to the laser power variation. Another strong justification of the kink position is the linewidth of BLS peaks, i.e. the ω-spread of the phonons, related to the phonon mean free path [45]. An apparent increase in the linewidth is observable after the kink (figure S9). The intercept (at $P = 0$ mW) of the fitted line before the kink defines the values of $c_{L,\|}$, $c_{L,\perp}$ at room temperature (i.e. without heating).

3.3. Band structure calculation

Figure 3(c) shows the sound velocity c_L as a function of the graphene volume fraction. The $c_{L,\|}$ increases from 2790 ± 50 to 3224 ± 60 m s^{-1} as the graphene volume fraction increases from 0.02 vol% to 0.51 vol%. The $c_{L,\|}$ of Gr(0.2)/PMMA is very close to the value of pure PMMA (2784 m s^{-1}) due to the extremely low graphene volume fraction. The $c_{L,\perp}$ for all specimens remains nearly the same to that of the PMMA as the direction normal to the Bragg stack [29, 30] is dominated by the polymer. From the BLS experiments, we directly obtained the longitudinal sound velocities of PMMA and the effective longitudinal sound velocities of the Gr/PMMA stacks. To determine the elastic moduli of the CVD graphene without the assumption of effective medium approximations [29], we conducted phononic band structure calculations by using the COMSOL Multiphysics package. Because of symmetry, we conducted two-dimensional (2D) simulations. The simulation domain consists of one layer of graphene and one layer of PMMA, with periodic boundary conditions applied on all four sides. The relevant parameters are listed in table 2. Specifically, we assumed the Poisson's ratio of graphene to be 0.17 [46] and considered the Young's modulus of the CVD graphene as an adjustable parameter. The elastic properties of the relatively thick PMMA layers were assumed to be the bulk PMMA values (Young's modulus = 6.272 GPa, Poisson's ratio = 0.333, based on our BLS measurements). By matching the measured effective longitudinal sound velocities of the Gr/PMMA stacks with the corresponding calculated values in the long wavelength limit, we determined the Young's modulus of the investigated CVD graphene to be 680 ± 16 GPa. Typical phononic band structures are shown in figures 4(a) and (b) for Gr(3.3)/PMMA in the cross-plane and in-plane directions, respectively. The periodicity-induced band folding is clearly seen in figure 4(a). For the band structure in the in-plane direction, we considered a small domain width of 1 nm to avoid band folding in the width direction. The slopes of the lowest two branches give the effective longitudinal and transverse sound velocities of the Gr(3.3)/PMMA stack, respectively. Figure 4(c) shows effective longitudinal and transverse sound velocities of the Gr/PMMA stacks as a function of the graphene volume fraction. It is interesting to note that as the graphene volume fraction increases, $c_{L,\|}$ increases, whereas $c_{L,\perp}$ and $c_{T,\|}$ ($\approx c_{T,\perp}$) remain nearly constant. At the limit of zero graphene volume fraction, $c_{L,\|} \approx c_{L,\perp}$ expectedly erasing the elastic anisotropy, $(c_{L,\|}/c_{L,\perp})^2$, of the PMMA rich Bragg stack, and c_L assumes the sound velocity of pure PMMA (black dashed line in figure 3(c)). Assuming an in-plane isotropy of graphene, we further obtained the shear modulus of graphene to be $G = E/[2(1 + \nu)] = 290 \pm 10$ GPa, which is in good agreement with the reported value (280 GPa at 0.4 K) for CVD graphene on silicon mechanical oscillator [47].

3.4. Uniaxial tensile modulus

Similar to our previous work [32], uniaxial tensile tests were conducted to evaluate the effect of CVD graphene on the elastic moduli of the Gr/PMMA hybrid Bragg stacks. In figure 5(a) exemplary stress–strain curves are presented for each volume fraction. The Young's modulus of each Gr/PMMA specimen was estimated from the linear part (0.1%–0.3% strain) of the stress–strain curves. For similar systems, it has been shown that even for a low thickness ratio of the two components, e.g. 0.044 vol% graphene, the modulus of elasticity of the composite shows a significant increase by 25% [32]. For the Gr(3.3)/PMMA, with the thickness of a PMMA layer being 100 nm, the Young's modulus increases to 4.4 ± 0.4 GPa, 150% higher than that of the bulk PMMA. The subsequent reduction in thickness of the matrix to 65 nm (Gr(5.1)/PMMA) yields an even larger increase of Young's modulus to 5.9 ± 0.4 GPa (a 250% increase). By using a simple rule-of-mixtures: $E_{Gr/PMMA} = E_m\phi_{PMMA} + E_f\,\phi_{Gr}$, where $E_{Gr/PMMA}$, E_{PMMA}, and E_{Gr} are the Young's moduli of the composite, PMMA, and graphene, respectively, and ϕ_{PMMA} and $\phi_{Gr} = 1 - \phi_{PMMA}$ are the volume fractions of the PMMA and graphene, respectively, and by extrapolating to 100% graphene volume fraction, the Young's modulus of the graphene was estimated to 817 ± 23 GPa (figure 5(b)).

4. Discussion and concluding remarks

We summarize the experimental Young's modulus of wrinkled graphene, as deduced from different experimental techniques, in figure 5(c) to visualize the comparison among them. AFM nanoindentation of CVD graphene with wrinkle height between 3 and 6 nm yielded to a Young's modulus of 167 ± 74 GPa [25], while a similar indentation technique with a gating voltage led to $E = 100 \pm 86$ GPa for CVD graphene with wrinkle heights of 3 nm [18]. However, nanoindentation itself can cause a large deformation in the out-of-plane direction, which may deteriorate the

Table 2. Parameters used in the phononic band structure calculations and Young's modulus of graphene from tensile tests.

Materials	Thickness (nm)	Width (nm)	Density (kg m^{-3})	Young's modulus (GPa) (computed)	Poisson's ratio	Young's modulus (GPa) (tensile test)
Graphene	0.335	1	2.267	680 ± 16	0.17 [46]	817 ± 23
PMMA	3.125–100	1	1.189	6.2 ± 0.2	0.333	1.8

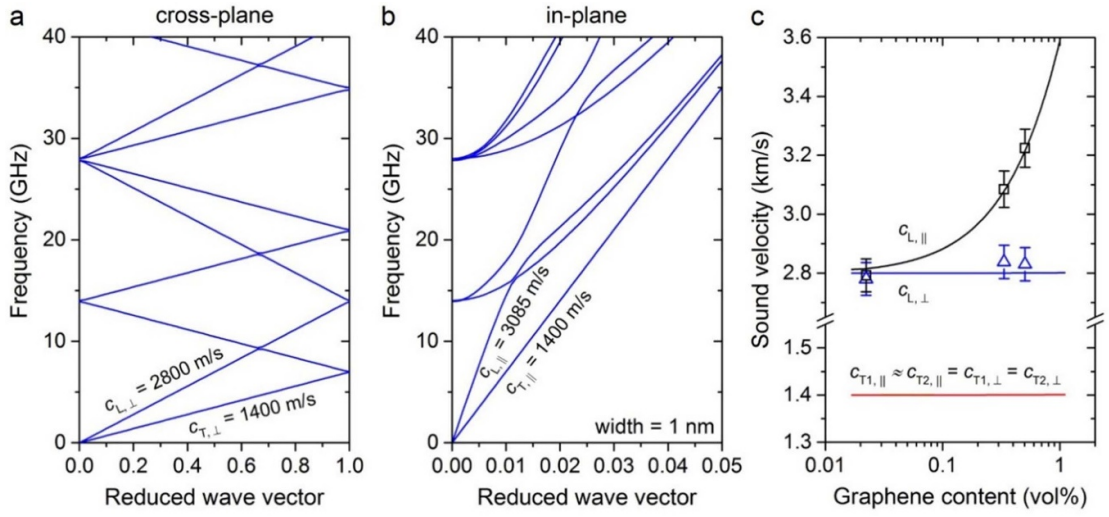

Figure 4. Calculated phononic band structure and effective sound velocities in Gr/PMMA Bragg stacks. The phononic band structures of Gr(3.3)/PMMA in the (a) cross-plane and (b) in-plane directions. The effective sound velocities of the lowest longitudinal and transverse branches in the long wavelength limit are indicated. (c) The effective longitudinal (L) and transverse (T) sound velocities of the Gr/PMMA stacks as a function of the graphene volume fraction.

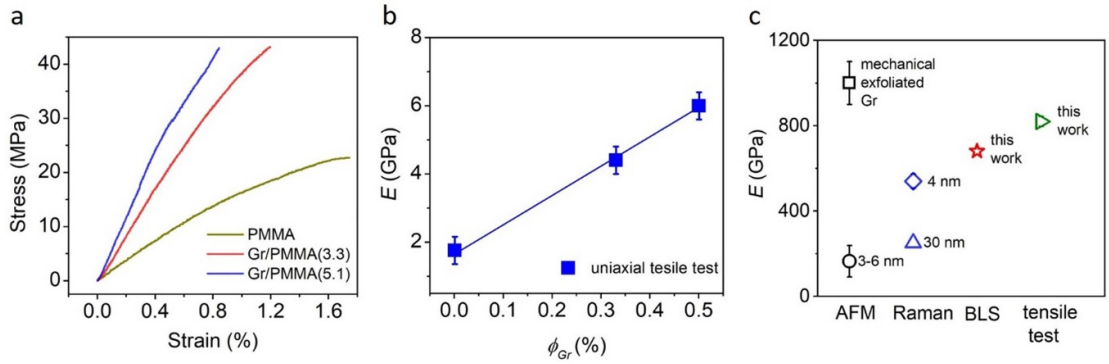

Figure 5. (a) Representative stress–strain curves of pure PMMA, Gr(3.3)/PMMA and Gr(5.1)/PMMA. (b) The Young's modulus in relation to the graphene volume fraction as obtained from tensile measurements. The solid is a linear-squares-fit to the experimental data of a slope of 8.15 GPa. (c) Experimental Young's moduli in CVD graphene of different wrinkle height by different techniques. Mechanically exfoliated graphene: [3]; CVD graphene having a wrinkle height of 3–6 nm: [25]; 4–8 nm: [48]; 30 nm: [24].

intrinsic stiffness of graphene. Yet, the strain distribution in wrinkled graphene is non-uniform, introducing large errors in the measured stiffness. Raman spectroscopy, which estimates the Young's modulus of a 2D material from the rate of the frequency shift of the characteristic peaks under strain, reported a Young's modulus of 250 GPa [24] for graphene with an average wrinkle height of ca. 30 nm. A more comprehensive summary of the Young's modulus of graphene, estimated by various experimental techniques, can be found in table S1.

The uniaxial tensile test is widely applied to measure the mechanical characteristics of the Bragg stacks such as the Young's modulus and the fracture stress/strain. For the specimens tested here the Young's modulus of CVD graphene was estimated to be 817 ± 23 GPa about 20% higher than 680 ± 16 GPa obtained from BLS. The main reason for this discrepancy is attributed to the straightening of the wrinkles upon the imposition of a tensile stress which results in higher Young's modulus than that estimated by the BLS method at zero strain [48]. A possible source

of error is also the linear extrapolation invoked in figure 5(b) which may not be holding to 100% volume fraction. We point out that in this work, the wrinkles in the CVD graphene were mainly introduced upon cooling of the CVD graphene on the copper substrate and the subsequent transfer process [49].

Unlike the methods mentioned above, BLS allows probing thermally excited phonons in a non-destructive manner. It is well-known that elastic properties are coupled with the acoustic sound velocities; therefore, accurate elastic moduli can be obtained by probing the effective sound velocity of the hybrid Bragg stacks. Our experiment provides a method for studying the elastic modulus of other two-dimensional materials, such as reduced graphene oxide (rGO) and graphene oxide (GO), which are commonly used fillers to reinforce the elastic properties of polymer-based composites. However, the wrinkle-induced softening effect in these materials has not yet been investigated. As a mature technique, the wet transfer can be easily employed to these 2D materials, and by probing the GO/PMMA or rGO/PMMA hybrid Bragg stacks using BLS, the longitudinal sound velocity can then be obtained. The elastic moduli can be subsequently calculated with the known Poisson's ratios. These results contribute to a better understanding of the elastic moduli of 2D materials and pave the way to accurately manipulating the elastic moduli of graphene nanolaminates.

Concluding, we report here a new approach to accessing the elastic modulus of the CVD graphene. By probing the effective phonon propagation of Gr/PMMA hybrid Bragg stacks using BLS and combining the phononic band structure calculations, we determined the Young's and shear moduli of the CVD graphene with a maximum height of 6 nm to be 680 $\pm$ 16 and 290 $\pm$ 10 GPa, respectively. In probing the thermal phonons, no strain was introduced, eliminating the possibility of strain hardening upon loading. This concept can be extended to determining the wrinkle-induced softening effect of other two-dimensional materials.

Data availability statement

The data that support the findings of this study are available upon reasonable request from the authors.

Acknowledgments

B L gratefully thanks the financial support from China Scholarships Council (No. 201906260224). Z W and G F acknowledge the financial support by ERC AdG SmartPhon (Grant No. 694977). Y C acknowledge the financial support by Shanghai Pujiang Program (Grant No. 20PJ1413800). C G and C P acknowledge the financial support of 'Graphene Core 3, GA: 881603—Graphene-based disruptive technologies', which is implemented under the EU-Horizon 2020 Research & Innovation Action. C G and C P are also thankful to Dr Anastasios Manikas for assisting with the Raman measurements, Dr Giovanna-Maria Pastore-Carbone for assisting with the nanocomposite fabrication and Dr George Trakakis for providing the CVD graphene samples. The authors declare that they have no known competing financial interests or personal relationships that could have appeared to influence the work reported in this paper.

Credit authorship contribution statement

Bohai Liu: Investigation, Formal analysis, Visualization, Writing—original Draft, Funding acquisition. Christos Pavlou: Resources, Formal analysis, Investigation, Writing—original Draft. Zuyuan Wang: Software, Writing—original Draft. Yu Cang: Methodology, Formal analysis. Costas Galiotis: Writing—review & editing, Supervision, Funding acquisition. George Fytas: Writing—review & editing, Supervision, Funding acquisition.

ORCID iDs

Bohai Liu https://orcid.org/0000-0002-6384-1953
Christos Pavlou https://orcid.org/0000-0001-7345-161X
Costas Galiotis https://orcid.org/0000-0001-8079-5488

References

[1] Balandin A A, Ghosh S, Bao W, Calizo I, Teweldebrhan D, Miao F and Lau C N 2008 Superior thermal conductivity of single-layer graphene *Nano Lett.* **8** 902–7
[2] Kim K S, Zhao Y, Jang H, Lee S Y, Kim J M, Kim K S, Ahn J H, Kim P, Choi J Y and Hong B H 2009 Large-scale pattern growth of graphene films for stretchable transparent electrodes *Nature* **457** 706–10
[3] Lee C, Wei X, Kysar J W and Hone J 2008 Measurement of the elastic properties and intrinsic strength of monolayer graphene *Science* **321** 385
[4] Novoselov K S, Geim A K, Morozov S V, Jiang D, Zhang Y, Dubonos S V, Grigorieva I V and Firsov A A 2004 Electric field effect in atomically thin carbon films *Science* **306** 666
[5] Liu F, Ming P and Li J 2007 Ab initio calculation of ideal strength and phonon instability of graphene under tension *Phys. Rev.* B **76** 064120
[6] Kuilla T, Bhadra S, Yao D, Kim N H, Bose S and Lee J H 2010 Recent advances in graphene based polymer composites *Prog. Polym. Sci.* **35** 1350–75
[7] Papageorgiou D G, Kinloch I A and Young R J 2017 Mechanical properties of graphene and graphene-based nanocomposites *Prog. Mater. Sci.* **90** 75–127
[8] Vlassiouk I, Polizos G, Cooper R, Ivanov I, Keum J K, Paulauskas F, Datskos P and Smirnov S 2015 Strong and electrically conductive graphene-based composite fibers and laminates *ACS Appl. Mater. Interfaces* **7** 10702–9
[9] Liu K and Wu J 2015 Mechanical properties of two-dimensional materials and heterostructures *J. Mater. Res.* **31** 832–44
[10] Yu Q, Lian J, Siriponglert S, Li H, Chen Y P and Pei S-S 2008 Graphene segregated on Ni surfaces and transferred to insulators *Appl. Phys. Lett.* **93** 113103

[11] Novoselov K S, Fal'ko V I, Colombo L, Gellert P R, Schwab M G and Kim K 2012 A roadmap for graphene *Nature* **490** 192–200
[12] Li X *et al* 2009 Large-area synthesis of high-quality and uniform graphene films on copper foils *Science* **324** 1312
[13] Zhang Y, Zhang L and Zhou C 2013 Review of chemical vapor deposition of graphene and related applications *Acc. Chem. Res.* **46** 2329–39
[14] Kim Y *et al* 2013 Strengthening effect of single-atomic-layer graphene in metal-graphene nanolayered composites *Nat. Commun.* **4** 2114
[15] Huang P Y *et al* 2011 Grains and grain boundaries in single-layer graphene atomic patchwork quilts *Nature* **469** 389
[16] Shekhawat A and Ritchie R O 2016 Toughness and strength of nanocrystalline graphene *Nat. Commun.* **7** 10546
[17] Pastore Carbone M G, Manikas A C, Souli I, Pavlou C and Galiotis C 2019 Mosaic pattern formation in exfoliated graphene by mechanical deformation *Nat. Commun.* **10** 1572
[18] Nicholl R J, Conley H J, Lavrik N V, Vlassiouk I, Puzyrev Y S, Sreenivas V P, Pantelides S T and Bolotin K I 2015 The effect of intrinsic crumpling on the mechanics of free-standing graphene *Nat. Commun.* **6** 8789
[19] Zhu W, Low T, Perebeinos V, Bol A A, Zhu Y, Yan H, Tersoff J and Avouris P 2012 Structure and electronic transport in graphene wrinkles *Nano Lett.* **12** 3431–6
[20] Li X, Zhu Y, Cai W, Borysiak M, Han B, Chen D, Piner R D, Colombo L and Ruoff R S 2009 Transfer of large-area graphene films for high-performance transparent conductive electrodes *Nano Lett.* **9** 4359–63
[21] Liu N, Pan Z, Fu L, Zhang C, Dai B and Liu Z 2011 The origin of wrinkles on transferred graphene *Nano Res.* **4** 996
[22] Jiang T, Wang Z, Ruan X and Zhu Y 2018 Equi-biaxial compressive strain in graphene: Grüneisen parameter and buckling ridges *2D Mater.* **6** 015026
[23] Shen X, Lin X, Yousefi N, Jia J and Kim J-K 2014 Wrinkling in graphene sheets and graphene oxide papers *Carbon* **66** 84–92
[24] Li Z, Kinloch I A, Young R J, Novoselov K S, Anagnostopoulos G, Parthenios J, Galiotis C, Papagelis K, Lu C-Y and Britnell L 2015 Deformation of wrinkled graphene *ACS Nano* **9** 3917–25
[25] Ruiz-Vargas C S, Zhuang H L, Huang P Y, Van Der Zande A M, Garg S, McEuen P L, Muller D A, Hennig R G and Park J 2011 Softened elastic response and unzipping in chemical vapor deposition graphene membranes *Nano Lett.* **11** 2259–63
[26] Ferrari A C and Basko D M 2013 Raman spectroscopy as a versatile tool for studying the properties of graphene *Nat. Nanotechnol.* **8** 235–46
[27] Frank O, Tsoukleri G, Riaz I, Papagelis K, Parthenios J, Ferrari A C, Geim A K, Novoselov K S and Galiotis C 2011 Development of a universal stress sensor for graphene and carbon fibres *Nat. Commun.* **2** 255
[28] Androulidakis C, Tsoukleri G, Koutroumanis N, Gkikas G, Pappas P, Parthenios J, Papagelis K and Galiotis C 2015 Experimentally derived axial stress–strain relations for two-dimensional materials such as monolayer graphene *Carbon* **81** 322–8
[29] Schneider D, Liaqat F, El Boudouti E H, El Hassouani Y, Djafari-Rouhani B, Tremel W, Butt H-J and Fytas G 2012 Engineering the hypersonic phononic band gap of hybrid Bragg stacks *Nano Lett.* **12** 3101–8
[30] Wang Z, Rolle K, Schilling T, Hummel P, Philipp A, Kopera B A F, Lechner A M, Retsch M, Breu J and Fytas G 2020 Tunable thermoelastic anisotropy in hybrid Bragg stacks with extreme polymer confinement *Angew. Chem., Int. Ed.* **59** 1286–94
[31] Hesami M, Gueddida A, Gomopoulos N, Dehsari H S, Asadi K, Rudykh S, Butt H J, Djafari-Rouhani B and Fytas G 2019 Elastic wave propagation in smooth and wrinkled stratified polymer films *Nanotechnology* **30** 045709
[32] Pavlou C, Pastore Carbone M G, Manikas A C, Trakakis G, Koral C, Papari G, Andreone A and Galiotis C Record EMI shielding behaviour of thin graphene/ PMMA nanolaminates in the THz range (in preparation)
[33] Cong X, Li Q-Q, Zhang X, Lin M-L, Wu J-B, Liu X-L, Venezuela P and Tan P-H 2019 Probing the acoustic phonon dispersion and sound velocity of graphene by Raman spectroscopy *Carbon* **149** 19–24
[34] Wang Z K, Lim H S, Ng S C, Özyilmaz B and Kuok M H 2008 Brillouin scattering study of low-frequency bulk acoustic phonons in multilayer graphene *Carbon* **46** 2133–6
[35] Nair R R, Blake P, Grigorenko A N, Novoselov K S, Booth T J, Stauber T, Peres N M R and Geim A K 2008 Fine structure constant defines visual transparency of graphene *Science* **320** 1308
[36] Androulidakis C, Koukaras E N, Parthenios J, Kalosakas G, Papagelis K and Galiotis C 2015 Graphene flakes under controlled biaxial deformation *Sci. Rep.* **5** 18219
[37] Anagnostopoulos G *et al* 2016 Mechanical stability of flexible graphene-based displays *ACS Appl. Mater. Interfaces* **8** 22605–14
[38] Wang G, Dai Z, Liu L, Hu H, Dai Q and Zhang Z 2016 Tuning the interfacial mechanical behaviors of monolayer graphene/PMMA nanocomposites *ACS Appl. Mater. Interfaces* **8** 22554–62
[39] Zhao Y, Liu X, Lei D Y and Chai Y 2014 Effects of surface roughness of Ag thin films on surface-enhanced Raman spectroscopy of graphene: spatial nonlocality and physisorption strain *Nanoscale* **6** 1311–7
[40] Khairy M, Amin N H and Kamal R 2017 Optical and kinetics of thermal decomposition of PMMA/ZnO nanocomposites *J. Therm. Anal. Calorim.* **128** 1811–24
[41] Koral C, Papari G, Carbone M G P, Pavlou C, Manikas A, Trakakis G, Galiotis C and Andreone A 2019 THz EMI shielding in graphene/PMMA multilayers *2019 44th Int. Conf. Infrared, Millimeter, and Terahertz Waves (IRMMW-THz)* p 1
[42] Voudouris P, Gomopoulos N, Le Grand A, Hadjichristidis N, Floudas G, Ediger M D and Fytas G 2010 Does Brillouin light scattering probe the primary glass transition process at temperatures well above glass transition? *J. Chem. Phys.* **132** 074906
[43] Thomas S, Ajith K M, Lee S U and Valsakumar M C 2018 Assessment of the mechanical properties of monolayer graphene using the energy and strain-fluctuation methods *RSC Adv.* **8** 27283–92
[44] Amirkhani M, Taschin A, Cucini R, Bartolini P, Leporini D and Torre R 2011 Polymer thermal and acoustic properties using heterodyne detected transient grating technique *J. Polym. Sci.* B **49** 685–90
[45] Mattarelli M, Vassalli M and Caponi S 2020 Relevant length scales in Brillouin imaging of biomaterials: the interplay between phonons propagation and light focalization *ACS Photonics* **7** 2319–28
[46] Cao G 2014 Atomistic studies of mechanical properties of graphene *Polymers* **6** 2404–32
[47] Liu X, Metcalf T H, Robinson J T, Houston B H and Scarpa F 2012 Shear modulus of monolayer graphene prepared by chemical vapor deposition *Nano Lett.* **12** 1013–7
[48] Lin Q-Y, Jing G, Zhou Y-B, Wang Y-F, Meng J, Bie Y-Q, Yu D-P and Liao Z-M 2013 Stretch-induced stiffness enhancement of graphene grown by chemical vapor deposition *ACS Nano* **7** 1171–7
[49] Huet B, Raskin J-P, Snyder D W and Redwing J M 2020 Fundamental limitations in transferred CVD graphene caused by Cu catalyst surface morphology *Carbon* **163** 95–104